frontiers in Environmental Chemistry

ORIGINAL RESEARCH
published: 23 November 2020
doi: 10.3389/fenvc.2020.591645

Layered MoS_2 Grown on Anatase TiO_2 {001} Promoting Interfacial Electron Transfer to Enhance Photocatalytic Evolution of H_2 From H_2S

Qing Cai[1,2], *Fang Wang*[1,2]*, *Jianglai Xiang*[2], *Meng Dan*[2], *Shan Yu*[2] and *Ying Zhou*[1,2]*

[1] State Key Laboratory of Oil and Gas Reservoir Geology and Exploitation, Southwest Petroleum University, Chengdu, China, [2] The Center of New Energy Materials and Technology, School of New Energy and Materials, Southwest Petroleum University, Chengdu, China

The treatment of hazardous hydrogen sulfide (H_2S) via photocatalysis technology has been known as one of the most promising green technologies. Photocatalytic production of hydrogen (H_2) from H_2S by two-dimensional (2D) semiconductor materials has gathered great attention owing to its large surface area and high catalytic activity. In this work, layered MoS_2 has been successfully grown on TiO_2 {001} surface to fabricate the 2D MoS_2/TiO_2 {001} composites for H_2 evolution from H_2S, which can be confirmed by the X-ray diffraction (XRD) and transmission electron microscopy (TEM) tests. Band structures and UV-Vis spectra provide important evidences that MoS_2 loading can significantly narrow the band gap and broaden the light absorbance into the visible light region. Electron transfer is obviously visualized at the interface of MoS_2/TiO_2, resulting in the built-in potential from TiO_2 to MoS_2, which is determined by the density functional theory (DFT) calculations and X-ray photoelectron spectroscopy (XPS) test. Consequently, the photo-induced electrons and holes are accumulated at the sides of TiO_2 and MoS_2 under the illumination, respectively, which largely promote the interfacial electron transfer and prolong the lifetime of photo-generated electrons that participate in the photocatalytic reactions of H_2 evolution from H_2S. This efficient separation of photo-induced carriers can be further proved by photoluminescence (PL) spectra, photocurrent responses, and electrochemical impedance spectra. As a result, the photocatalytic activity of H_2 evolution is largely increased by 9.4 times compared to the pristine TiO_2. This study could offer a new and facile way to design highly efficient 2D photocatalysts for the application of H_2S treatment.

Keywords: photo-splitting of H_2S, H_2, MoS_2/TiO_2 {001}, electron transfer, DFT

OPEN ACCESS

Edited by:
Dengsong Zhang,
Shanghai University, China

Reviewed by:
Likun Pan,
East China Normal University, China
Yuechang Wei,
China University of Petroleum, China

***Correspondence:**
Fang Wang
wangfnjust@163.com
Ying Zhou
yzhou@swpu.edu.cn

Specialty section:
This article was submitted to Catalytic Remediation, a section of the journal Frontiers in Environmental Chemistry

Received: *05 August 2020*
Accepted: *08 September 2020*
Published: *23 November 2020*

Citation:
Cai Q, Wang F, Xiang J, Dan M, Yu S and Zhou Y (2020) Layered MoS_2 Grown on Anatase TiO_2 {001} Promoting Interfacial Electron Transfer to Enhance Photocatalytic Evolution of H_2 From H_2S. Front. Environ. Chem. 1:591645. doi: 10.3389/fenvc.2020.591645

INTRODUCTION

Hydrogen sulfide (H_2S), as a highly toxic and corrosive pollutant, has been massively discharged from the natural gas extraction and oil refineries, which causes a serious threat on the air environment and human health with a fatal concentration over 700 ppm in the air. Thus, H_2S treatment has become a long-standing issue that attracts great worldwide attention. Photocatalysis

technology, directly driven by the solar energy, has been considered to be an effective new-generation green technologies (Liu et al., 2012, 2018, 2019; Wang et al., 2012; Ren et al., 2020). More importantly, clean energy H_2 can be produced during the photo-splitting of H_2S, which can alleviate the pressing global energy crisis and the environmental problems from the perspective of renewable resource utilization (Dan et al., 2017, 2019a,b; Xiang et al., 2019). Recently, anatase TiO_2 nanosheet with exposed {001} facets has been proven to be a promising candidate for photocatalytic production of H_2 because of the high reactivity and non-toxic features (Altomare et al., 2018; Chen et al., 2018; Ge et al., 2019; Yu et al., 2019), and the photocatalytic mechanism of H_2 production from H_2S on anatase TiO_2 {001} was reported in our previous work (Cai et al., 2020). However, the wide band gap and high charge recombination enormously restrict its photocatalytic activity. Surface modification via noble metal loading such as Au and Ag is usually applied to design TiO_2-based photocatalysts to pursue highly efficient production of H_2 (Zhao et al., 2018; Wang et al., 2019; Sharma et al., 2020). The high cost and limited storage of noble metals are of serious concerns. Thus, it deserves to develop economy and efficient methods to modify TiO_2 to achieve a high conversion activity of H_2. Particularly, two-dimensional (2D) layered MoS_2, as a non-noble metal catalyst, has attracted great attention because of the ability to capture electrons with the unique layered sandwich structure (Sun et al., 2018; Li Y. et al., 2019). Furthermore, various researches have reported that the layered MoS_2 can act as an excellent cocatalyst for both photocatalytic and electrocatalytic evolution of H_2 owing to the abundantly exposed edges (Li et al., 2011; Kibsgaard et al., 2012; Chang et al., 2014). It was shown that the fabrication of an MoS_2/TiO_2 heterostructure can largely promote the H_2 production from H_2O due to the much lower reaction energy barriers along the hydrogen evolution reaction paths (Tang et al., 2017). Other researchers also found that the MoS_2 nanosheets grown on TiO_2 could produce more active edges, and the efficient separation of the photo-generated carries resulted in the excellent H_2 production from H_2O (Liu Q. et al., 2013; Zhang et al., 2015). However, the promising MoS_2/TiO_2 composite has been barely applied to H_2 evolution from H_2S as yet, and the enhanced photocatalytic mechanism of H_2 production deserves in-depth study.

In the present study, a facile two-step hydrothermal method has been adopted to prepare the layered MoS_2 grown on TiO_2 {001}. The morphology, component, optical properties, and interfacial electron transfer of the fabricated MoS_2/TiO_2 {001} are investigated in-depth by experimental tests such as transmission electron microscopy (TEM), X-ray photoelectron spectroscopy (XPS), and photoluminescence (PL) spectra as well as the density functional theory (DFT) calculations.

EXPERIMENTAL METHOD AND THEORETICAL CALCULATION

TiO_2 {001} Synthesis

TiO_2 synthesis adopts a traditional hydrothermal method with the shape control agent HF (Yuan et al., 2016; Yang et al., 2018), as has been successfully prepared in our previous work (Yu et al., 2016). First, 3.75 ml of butyl titanate and 0.6 ml of HF is placed into a 15-ml of complete dried Teflon-lined stainless-steel autoclave. Then the autoclave is sealed and placed in an electric oven held at 200°C for 24 h. Then, 0.1 M NaOH solution is applied to neutralize the F^- by stirring washing precipitates for 2 h after autoclave cooling to room temperature. Next, the precipitates are separated by vacuum filtration, washed with ultrapure water and alcohol several times until pH 7. Finally, the precipitates are dried overnight at 60°C in a vacuum oven.

Preparation of MoS_2/TiO_2 {001} (MoS_2/TiO_2) Composites

A two-step hydrothermal method is conducted to prepare the MoS_2/TiO_2 composites. First, 200 mg of TiO_2 powder is placed into a 50-ml Teflon-lined stainless-steel autoclave containing 25 ml of ultrapure water. Then, 7.7 mg ammonium molybdate and 72.6 mg thiourea are added into the above autoclave. After stirring for 15 min, the autoclave is heated at 180°C for 24 h. The final powder is washed several times with ultrapure water and ethanol and dried at 60°C under a vacuum environment. Finally, the prepared composite is named as MoS_2/TiO_2-0.5. Other composites with 15.4, 30.8, and 46.2 mg of ammonium molybdate and 145.2, 290.4, and 435.6 mg of thiourea are ordered as MoS_2/TiO_2-1, MoS_2/TiO_2-2, and MoS_2/TiO_2-3.

Material Characterization

The powder structure and crystal phase of the samples are determined by X'pert powder X-ray diffraction (XRD) radiation operated at 40 kV/40 mA. UV-Vis spectrum is recorded at room temperature by Shimadzu UV-2600 spectrophotometer equipped with a double integrating sphere, and $BaSO_4$ is used as the reflectance standard. XPS (Thermo ESCALAB 250XI) measurement is conducted to investigate the surface chemical environment of samples referenced to the C 1s level at 284.8 eV. TEM (JEM 2100F) tests are carried out to investigate the microstructure of samples. Energy dispersive X-ray spectroscopy (EDS) is used to obtain an elemental mapping. The photoluminescence (PL) spectra are tested with a fluorescence spectrophotometer (excitation at 340 nm). The progress of photocatalytic activity measurements is referenced to our previous work (Cai et al., 2020).

Theoretical Calculations

2D MoS_2/TiO_2 configuration is built with relaxed rectangular $5 \times \sqrt{3}$ MoS_2 monolayers and a relaxed four-layer 3×1 anatase TiO_2 {001} surface. The crystal lattice match can be quantified by $\delta = |a_{001} - a_g|/a_{001}$ (Lin et al., 2017), where a_{001} is the lattice constant of the relaxed anatase TiO_2 {001} surface, and a_g is the lattice constant of the relaxed MoS_2 monolayer. The calculated δ for the lattice parameters a and b are 2.8 and 2.1% for the MoS_2/TiO_2, respectively, which are in a reasonable and acceptable range. The bottom Ti and O atoms of MoS_2/TiO_2 composites are fixed during the calculations, while other atoms are fully relaxed to simulate the interaction between TiO_2 surface and MoS_2 sheet. A vacuum space of 20 Å is applied to construct MoS_2/TiO_2 composites in order to avoid interactions between the periodic neighboring slabs. The

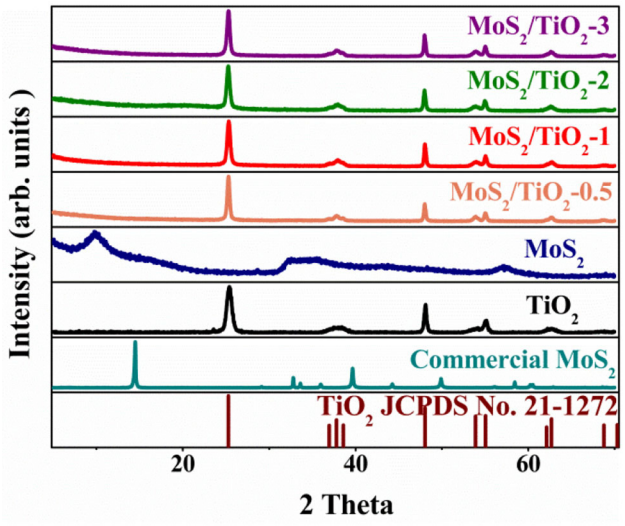

FIGURE 1 | X-ray diffraction (XRD) spectra of as-prepared samples.

Vienna *ab initio* simulation package (VASP) with the GGA-PBE exchange-correlation method is adopted in all calculation processes (Kresse and Furthmüller, 1996; Kresse and Joubert, 1999). The PAW method is used to describe the electron–ion interactions for Ti, O, Mo, and S atoms. Furthermore, to correct the strong interaction of Ti 3d and Mo 4d electron orbital, the coulombic interaction U and exchange energy J parameters are set according to the previous theoretical study (Cao et al., 2014). **Supplementary Figure 1** showed the MoS_2/TiO_2 structure after geometry optimization. To study the structural stability of the MoS_2/TiO_2 composites, the interface binding energy (E_b) is obtained in Equation (1):

$$E_b = E_{TM} - E_M - E_T \quad (1)$$

where E_{TM}, E_M, and E_T are the total energies of relaxed MoS_2/TiO_2 composites, relaxed MoS_2, and TiO_2 surface.

Interfacial electron transfer between TiO_2 and MoS_2 can be investigated by the following Equation (2):

$$\Delta_\rho = \rho_{TM} - \rho_M - \rho E_T \quad (2)$$

where ρ_{TM}, ρ_M, and ρ_T are the charge densities of the MoS_2/TiO_2 composites, MoS_2 structure, and TiO_2 surface, respectively. Furthermore, adsorption energy (E_{ad}) is used to describe the interaction between surface and adsorbed molecule, and the more negative E_{ad} value meant a more stable reaction progress, which can be calculated by the following Equation (3):

$$E_{ad} = E_{adsorbate/surface} - E_{adsorbate} - E_{surface} \quad (3)$$

$E_{adsorbate/surface}$ represented the energy of the surface with adsorbed molecule, $E_{adsorbate}$ is the energy of solitary adsorbed molecule, and $E_{surface}$ is the energy of surface.

Work function (Φ) is calculated by the energy difference between the electrostatic potential of the vacuum level (E_{vac}) and the Fermi energy (E_F) (Toroker et al., 2011).

$$\Phi = E_{vac} - E_F \quad (4)$$

RESULT AND DISCUSSION

Morphology Analysis

Crystallographic structures of prepared TiO_2, MoS_2, and MoS_2/TiO_2 composites are characterized by powder XRD (**Figure 1**). Prepared TiO_2 is indexed to the anatase phase (JCPDS No. 12-2172). It is worth noting that ammonium ions from ammonium molybdate hydrolysis can easily inlayer into MoS_2, which results in (002) peak obvious shifting to 9.65° (Liu et al., 2015; Zhang et al., 2017). Furthermore, no obvious MoS_2 peaks occur on MoS_2/TiO_2, which may be due to the small loading amount and its high dispersion on the surface of TiO_2 (Yuan et al., 2016).

Photocatalytic Activity of TiO_2 and MoS_2/TiO_2 Composites

Figure 2 shows the photocatalytic H_2 production from H_2S of pristine TiO_2 and MoS_2/TiO_2 composites. As shown in **Figure 2A**, TiO_2 reveals a poor photocatalytic hydrogen evolution activity. Remarkably, all the MoS_2/TiO_2 composites exhibit a higher photocatalytic performance than the pristine TiO_2. In particular, MoS_2/TiO_2-2 possesses the highest H_2 evolution rate compared to TiO_2, which is about 9.4 times higher than TiO_2 (**Figure 2B**). Meanwhile the H_2 evolution rate is close to the previous report (Zhang et al., 2020) using the different MoO_2/MoS_2 composites as the photocatalyst with the same reaction media (**Supplementary Table 1**). The stable growth trend of H_2 evolution indicated that H_2S decomposed on MoS_2/TiO_2 is steady in an H_2S environment. Meanwhile, the variation of E_{ad} also can reveal the decomposition stability of H_2S. The E_{ad} values for the decomposed fragments of H_2S including HS–H, H–S–H, and H_2-S on the TiO_2 surface are −2.65, −1.72, and −0.44 eV, while that on the MoS_2/TiO_2 surface are −2.69, −1.77, and −0.51 eV, respectively (**Figures 2C,D**). The more negative E_{ad} value suggests that the decomposition of H_2S fragments on the MoS_2/TiO_2 surface are more stable, which can be responsible for the high and stable photocatalytic activity. According to the activity results, the following characterizations including the crystal structure, morphology, surface chemical state, and optoelectronic properties are investigated for MoS_2/TiO_2-2 with the optimal activity as well as pristine TiO_2 for comparison.

Microstructure Analysis

To gain an intuitional understanding of the interface morphological structure between MoS_2 and TiO_2, the morphology of the TiO_2 and MoS_2/TiO_2-2 nanostructures is thoroughly investigated by the TEM test. Meanwhile, EDS mapping of MoS_2/TiO_2-2 in **Supplementary Figure 2** revealed four kinds of elements including Ti, O, Mo, and S. This result suggested that Mo and S have loaded on TiO_2. The TEM image

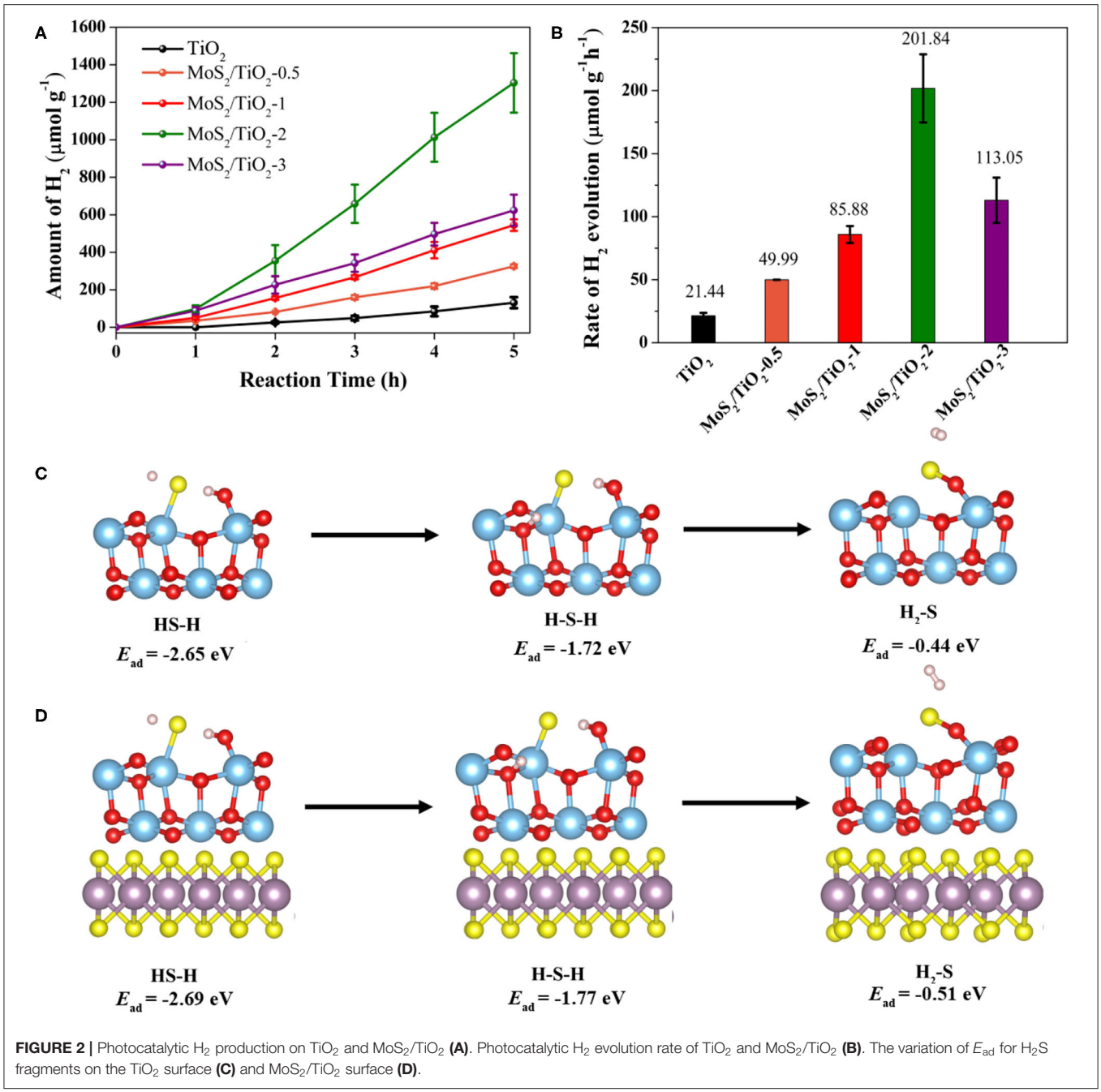

FIGURE 2 | Photocatalytic H_2 production on TiO_2 and MoS_2/TiO_2 **(A)**. Photocatalytic H_2 evolution rate of TiO_2 and MoS_2/TiO_2 **(B)**. The variation of E_{ad} for H_2S fragments on the TiO_2 surface **(C)** and MoS_2/TiO_2 surface **(D)**.

of MoS_2/TiO_2-2 photocatalyst presented in **Figure 3c** shows that the composite exhibits a morphology similar to ultrathin pure TiO_2 nanosheet (**Figure 3a**). In addition, nanolayer materials are remarkably cladding with TiO_2 nanosheet. HRTEM is applied to explore the morphology structure of prepared photocatalysts. As displayed in **Figure 3b**, the HRTEM image recorded from a single nanosheet clearly shows that the sample is made up of anatase TiO_2 nanosheets with lattice fringes of 0.35 and 0.24 nm, which are attributed to the (101) plane and (001) plane of anatase TiO_2, respectively (Zhou et al., 2013; Yang et al., 2018). Compared to ultrathin pure TiO_2, the HRTEM image of MoS_2/TiO_2-2 (**Figures 3c,d**) indicates the extra crystal lattice fringes of 0.63 nm, which are attributed to the (002) plane of the nanolayer MoS_2 (Liu et al., 2017).

Electronic Properties and Chemical Valence

According to the above analysis, MoS_2 loading has little effect on the morphological structure of TiO_2. To explore the reason for the high photocatalytic activity, the interfacial interaction between TiO_2 and MoS_2 are further studied. As shown in **Figure 4A**, the band gap (E_g) of TiO_2, MoS_2, and MoS_2/TiO_2

is 2.77, 1.60, and 1.54 eV, respectively. The introduction of MoS_2 largely reduced E_g by 1.23 eV compared to TiO_2, and the narrowed E_g can broaden the light absorption into the visible light region and make the electron excitation much easier. **Figure 4B** illustrates that the valence band and conduction band of MoS_2/TiO_2 are interlaced consisted by TiO_2 and MoS_2, resulting in the interfacial electron transfer from O 2p of TiO_2 to Mo 4d of MoS_2. The obvious peaks of O 2p and Mo 4d orbits locate at the same energy level at the top of valence bands, and this orbital hybridization features indicate the strong interface interaction between TiO_2 and MoS_2.

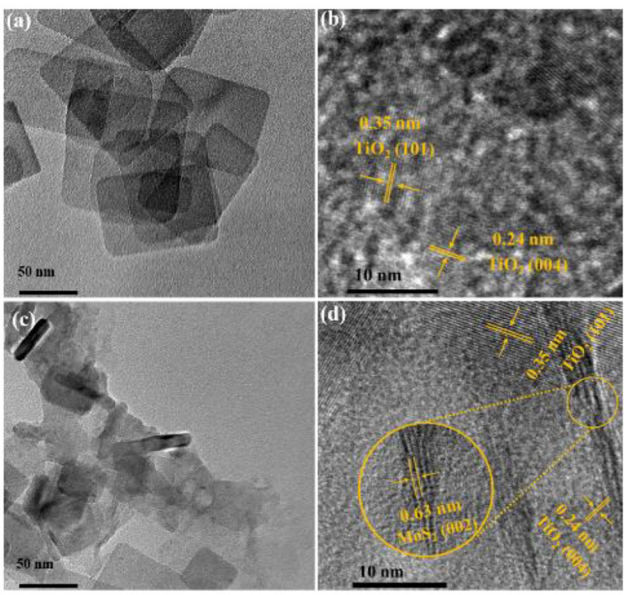

FIGURE 3 | Transmission electron microscopy (TEM) and HRTEM spectra of TiO_2 **(a,b)** and MoS_2/TiO_2-2 **(c,d)**.

The chemical valence state of Ti 2p, O 1s, Mo 3d, and S 2p are analyzed by X-ray photoelectron spectroscopy (XPS), which can examine the changes in valence states. The chemical valence state of Ti 2p is shown in **Figure 5A**. The two peaks at 464.4 and 458.8 eV are ascribed to Ti $2p_{1/2}$ and $2p_{3/2}$ with +4 valence from TiO_2, which are in good agreement with the previous report (Yang, 2018). O 1s spectrum is given in **Figure 5B**; peak separation for TiO_2 shows two kinds of oxygen with binding energies of 529.7 and 530.2 eV, which are assigned to the O lattice of TiO_2 and oxygen coordination with Ti species (Gao et al., 2015; Li X. et al., 2019). In comparison, Ti 2p and O 1s of MoS_2/TiO_2-2 show an evident shift to higher energy, suggesting electron depletion or transfer at the composite interface, which is consistent with the DOS result. **Figure 5C** shows the Mo 3d valence state of MoS_2/TiO_2-2 composites. The typical peaks of 228.1 and 232.3 eV ensure the appearance Mo^{4+} of MoS_2 (Shuxian et al., 1986; Woo et al., 1992). Meanwhile, peaks at 231.1 and 234.9 eV are consistent with the Mo^{4+} of MoO_2 (Brox and Olefjord, 1988), which is due to the higher electronegativity of O (Bao et al., 2016). Furthermore, peaks at 161.2 and 162.5 eV demonstrate the existence of S^{2-} in **Figure 5D**, suggesting the formation of MoS_2 (Liu L. et al., 2013; Song et al., 2018). In addition, sulfur peak at 164.3 eV means some sulfur ions may be reduced in the reaction process (Zeng et al., 2019).

According to DOS analysis, it can be found that some electron transfer from TiO_2 to MoS_2 at the interface of MoS_2/TiO_2-2 composites, thus, causing a strong interfacial interaction. Furthermore, the electron transfer behavior at the interface is further explored by charge density difference maps as shown in **Figure 6**. A large amount of charge redistribution at MoS_2 side may be induced by the strong interaction between TiO_2 and MoS_2. Furthermore, there are 0.10 e electrons flowing from TiO_2 to MoS_2, which is larger than the previous report

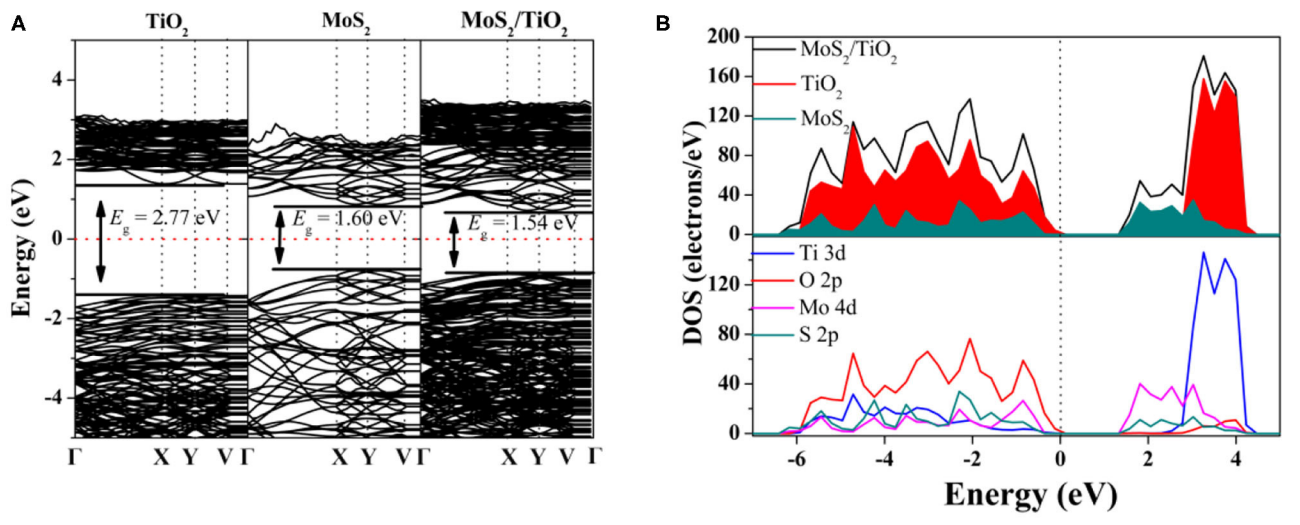

FIGURE 4 | Band structures **(A)** and DOS **(B)** of TiO_2, MoS_2, and MoS_2/TiO_2.

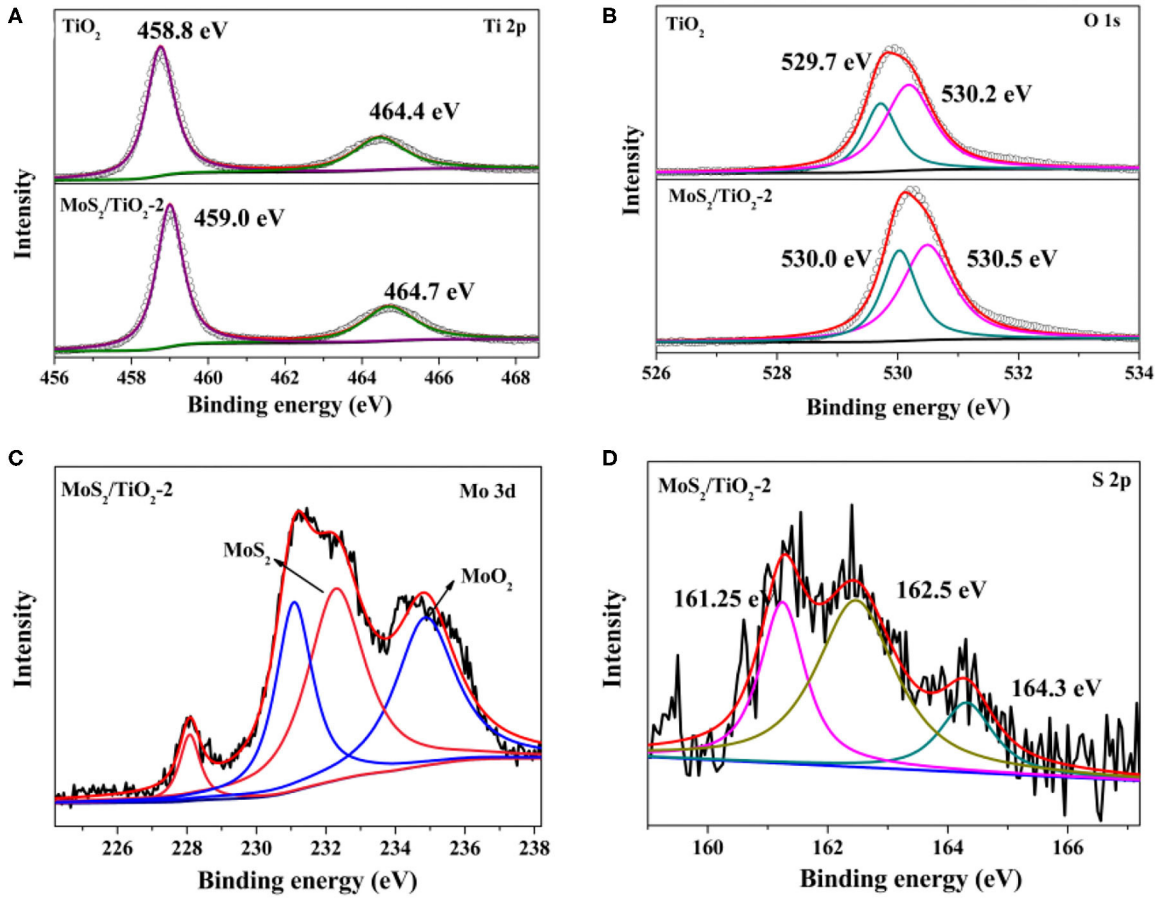

FIGURE 5 | The chemical valence state of **(A)** Ti 2p, **(B)** O 1s, **(C)** Mo 3d, and **(D)** S 2p.

(electron transfer quantity is 0.035 e) (Cao et al., 2014). A built-in electric field with the direction from TiO_2 to MoS_2 will form at the interface after the redistribution of the electron reaches an equilibrium state. The same phenomenon also can be found in DOS and XPS, which suggests a strong interfacial interaction between TiO_2 and MoS_2. Furthermore, the binging energy (E_b) of MoS_2/TiO_2 is −0.07 eV. The more negative E_b value means the more stable constructed structure and the stronger interface bonding at the composite interface (Bhowmik et al., 2007; Rybolt et al., 2007). As a result, MoS_2/TiO_2 can provide more electrons to participate in the reaction under light irradiation, and the electron transfer quantity of H_2-S fragments on the surface (**Supplementary Figure 3**) also reveals the same result that the electron transfer quantity has increased by 0.01 e on the MoS_2/TiO_2 surface. At the same time, the interfacial photo-generated carrier transfer mechanism (**Figure 7**) illustrates the interfacial electron migration route under the illumination. According to the electrostatic potential in vacuum, the Φ value of TiO_2 and MoS_2/TiO_2 is 4.52 and 5.23 eV, respectively (**Supplementary Figure 4**). Meanwhile, due to the more negative conduction band of TiO_2 and the more positive valence band of MoS_2, electrons and holes are consumed at the TiO_2 conduction band and MoS_2 valence band to participate in the redox reaction. Correspondingly, electrons and holes are accumulated at the MoS_2 conduction band and TiO_2 valence band, respectively. Because of the existence of the built-in electric field, the electrons at the TiO_2 conduction band cannot transfer to the MoS_2 conduction band, and holes at the MoS_2 valence band cannot transfer to the TiO_2 valence band. As a result, the translation direction of the electrons at the interface is from the MoS_2 conduction band to the TiO_2 valence band under light irradiation. Finally, the interfacial electron transfer mechanism prevents the electron from transferring from the conduction band of TiO_2 to the valence band of TiO_2 and results in a Z-scheme heterojunction. In other words, the interfacial electron transfer mechanism promotes the separation of electrons–holes and prolonged the lifetime of electrons, which facilitates the electrons accumulated at the conduction band of TiO_2 to take part in the photocatalytic reactions. This plays an important role in enhancing the H_2 production.

Optical and Photoelectric Properties

The UV-vis spectrum (**Figure 8A**) illustrates that the absorption edges of MoS_2/TiO_2 have obviously shifted to the visible light area compared with pure anatase TiO_2 nanosheets. This phenomenon suggests that the MoS_2/TiO_2 band gap is smaller

than TiO_2 and brings the light absorbance broadening to the visible-light area, which is consistent with the band structure result that MoS_2/TiO_2 with the narrower E_g should have a better light response. Meanwhile, the broader light absorbance of MoS_2/TiO_2 can produce more photo-generated electrons and boost the photocatalytic reaction. The photoluminescence (PL) emission spectra (**Figure 8B**) are further used to investigate the behavior of photo-generated carriers. Remarkably, the lower emission peak intensity of MoS_2/TiO_2 proves a higher photo-generated carrier separation efficiency and provides more photo-generated electrons to participate in H_2 evolution reaction as possible, which has the same result with interfacial electron transfer mechanism. **Figure 8C** presents the periodic on/off photocurrent response of TiO_2 and MoS_2/TiO_2-2 under irradiation with a 300-W Xe lamp. TiO_2 generates a relatively low photocurrent density with a value of 0.25 $\mu A\ cm^{-2}$. The photocurrent density of MoS_2/TiO_2-2 significantly increases after MoS_2 loading on the surface of TiO_2 nanosheets. MoS_2/TiO_2-2 shows the highest photocurrent density of 0.79 μAcm^{-2}, which is about three times higher than that of TiO_2. This conclusively demonstrates that the separation efficiency of photo-generated charge carriers can be significantly enhanced by MoS_2 existing on MoS_2/TiO_2 under light irradiation, which may be caused by the interfacial electron transfer mechanism. Furthermore, MoS_2/TiO_2-2 displays the lowest electrochemical impedance under light irradiation, giving a fast carrier separation performance (**Figure 8D**). As a result, the growth of the layered MoS_2 on TiO_2 cannot only promote the photo-generated carrier separation but also stimulates photo-generated electron transfer.

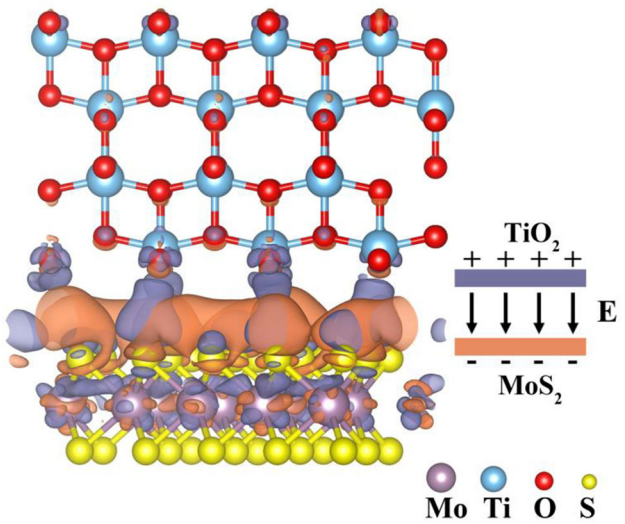

FIGURE 6 | The charge density difference map (0.0002 electrons/Å^3) of MoS_2/TiO_2. Orange and violet represent electron accumulation and depletion, respectively.

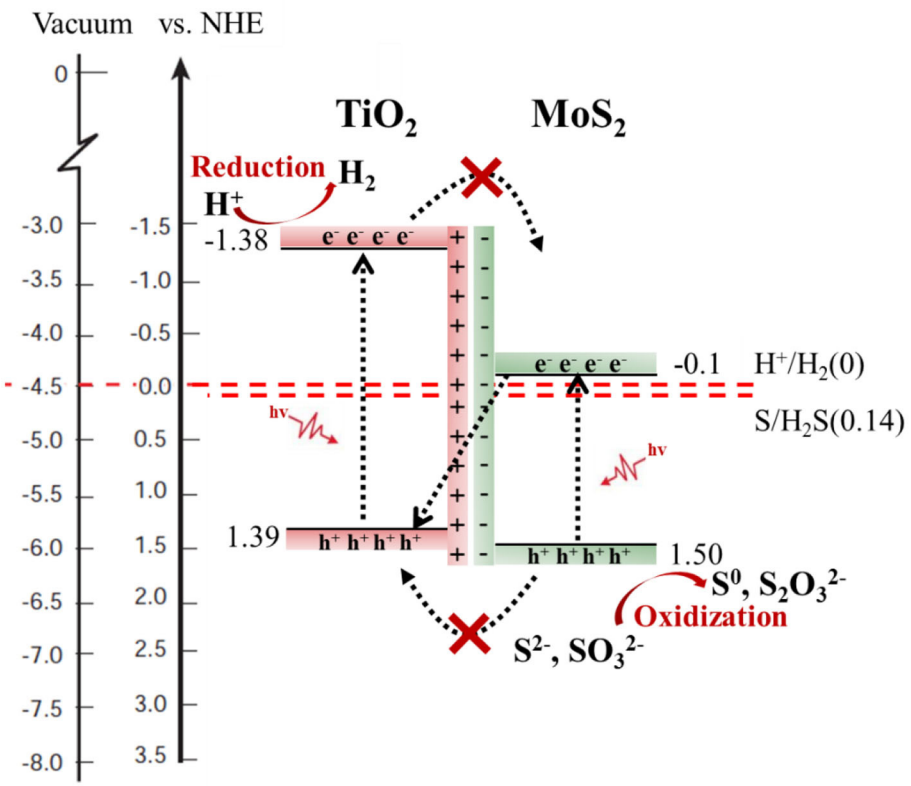

FIGURE 7 | Interfacial photo-generated carrier transfer mechanism.

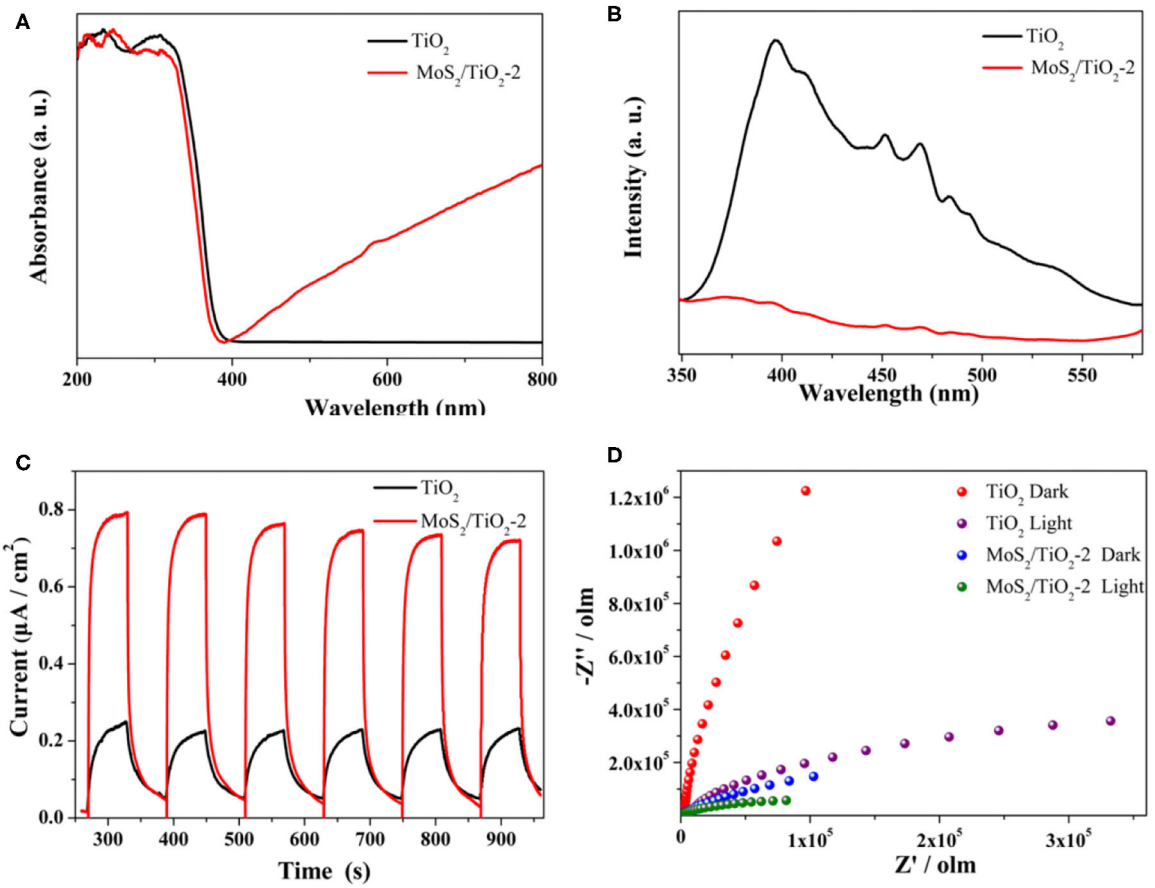

FIGURE 8 | UV-vis absorption spectrum **(A)**. Photoluminescence (PL) spectrum of as-prepared samples **(B)**. Transient photocurrent responses of TiO_2 and MoS_2/TiO_2-2 **(C)**. Electrochemical impedance spectrum for TiO_2 and MoS_2/TiO_2-2 with the light on or off **(D)**.

According to the above analysis, the effects of the layered MoS_2 loading on TiO_2 {001} can be ascribed to the following several points. First, loading MoS_2 can enhance the photocatalytic H_2 evolution. MoS_2/TiO_2-2 shows about 9.4 times H_2 evolution rate than TiO_2. The stable growth trend of H_2 evolution indicated that H_2S decomposing on MoS_2/TiO_2 is steady in the H_2S environment. Second, the interfacial electron transfer mechanism can prolong the life-time photo-generated electrons and increased the possibility of electrons to take part in H_2 evolution reaction, which can result in high photocatalytic activity for MoS_2/TiO_2. The band structure shows that the narrower band gap of MoS_2/TiO_2 can broaden the light response into the visible light area. Meanwhile, the broader light response area means more photo-generated electron production, which is beneficial to the photocatalytic reaction. Furthermore, the lower PL intensity and higher photocurrent response of MoS_2/TiO_2 caused by the interfacial electron transfer mechanism reveals the high efficiency of photo-generated carrier separation, which can be the key factor for high H_2 evolution.

CONCLUSION

This work reports the fabrication of 2D MoS_2/TiO_2 via loading of the layered MoS_2 on TiO_2 {001} for the photocatalytic conversion of H_2 from H_2S. The introduction of MoS_2 greatly narrows the E_g and causes the admirable light absorbance in the visible light area, which is in good agreement with the UV-Vis tests. Moreover, obvious electron transfer is visualized at the interface of MoS_2/TiO_2, resulting in the built-in potential from TiO_2 to MoS_2, which is determined by DFT calculations and XPS test. Significantly, the interfacial electron transfer largely reduces the photo-generated carrier recombination and prolongs the lifetime of photo-generated electrons, which can be determined by the lower PL intensity and higher photocurrent response. Consequently, the photoactivity of H_2 evolution is significantly improved from 21.44 to 201.84 $\mu mol\ g^{-1}\ h^{-1}$. This study can provide new insights into designing efficient 2D photocatalysts to meet high H_2 evolution from H_2S by photocatalysis technology.

DATA AVAILABILITY STATEMENT

The raw data supporting the conclusions of this article will be made available by the authors, without undue reservation.

AUTHOR CONTRIBUTIONS

QC wrote the original draft. FW conceptualized, wrote, reviewed, and edited the manuscript. JX made the formal analysis. MD and SY were responsible for visualization and investigation. YZ wrote, reviewed, edited, and supervised the study. All authors contributed to the article and approved the submitted version.

FUNDING

This research was financially supported by the National Natural Science Foundation of China (U1862111), CAS Light of West China Program and Open Fund of State Key Laboratory of Oil, Gas Reservoir Geology and Exploitation (Southwest Petroleum University) (PLN 201802), and Open Fund of State Key Laboratory of Industrial Vent Gas Reuse (SKLIVGR-SWPU-2020-05).

SUPPLEMENTARY MATERIAL

The Supplementary Material for this article can be found online at: https://www.frontiersin.org/articles/10.3389/fenvc.2020.591645/full#supplementary-material

REFERENCES

Altomare, M., Nguyen, N. T., Hejazi, S., and Schmuki, P. (2018). A cocatalytic electron-transfer cascade site-selectively placed on TiO_2 nanotubes yields enhanced photocatalytic H_2 evolution. *Adv. Funct. Mater.* 28:1704259. doi: 10.1002/adfm.201704259

Bao, T., Yin, W., Zheng, X., Zhang, X., Yu, J., Dong, X., et al. (2016). One-pot synthesis of PEGylated plasmonic MoO_{3-x} hollow nanospheres for photoacoustic imaging guided chemo-photothermal combinational therapy of cancer. *Biomaterials* 76, 11–24. doi: 10.1016/j.biomaterials.2015.10.048

Bhowmik, R., Katti, K. S., and Katti, D. (2007). Molecular dynamics simulation of hydroxyapatite–polyacrylic acid interfaces. *Polymer* 48, 664–674. doi: 10.1016/j.polymer.2006.11.015

Brox, B., and Olefjord, I. (1988). ESCA studies of MoO_2 and MoO_3. *Surf. Interface Anal.* 13, 3–6. doi: 10.1002/sia.740130103

Cai, Q., Wang, F., He, J., Dan, M., Cao, Y., Yu, S., et al. (2020). Oxygen defect boosted photocatalytic hydrogen evolution from hydrogen sulfide over active {001} facet in anatase TiO_2. *Appl. Surf. Sci.* 517:146198. doi: 10.1016/j.apsusc.2020.146198

Cao, L., Wang, R., Wang, D., Xu, L., and Li, X. (2014). Enhanced visible light photocatalytic activity for the hybrid MoS_2/anatase TiO_2(001) nanocomposite: a first-principles study. *Chem. Phys. Lett.* 612, 285–288. doi: 10.1016/j.cplett.2014.08.048

Chang, K., Mei, Z., Wang, T., Kang, Q., Ouyang, S., and Ye, J. (2014). MoS_2/graphene cocatalyst for efficient photocatalytic H_2 evolution under visible light irradiation. *ACS Nano* 8, 7078–7087. doi: 10.1021/nn5019945

Chen, W., Yu, S., Zhong, Y., Fan, X., Wu, L., and Zhou, Y. (2018). Effect of electron transfer on the photocatalytic hydrogen evolution efficiency of faceted TiO_2/CdSe QDs under visible light, *N. J. Chem.* 42, 4811–4817. doi: 10.1039/C8NJ00180D

Dan, M., Wei, S., Doronkin, D. E., Li, Y., Zhao, Z., Yu, S., et al. (2019a). Novel MnS/$(In_xCu_{1-x})_2S_3$ composite for robust solar hydrogen sulphide splitting via the synergy of solid solution and heterojunction. *Appl. Catal. B Environ.* 243, 790–800. doi: 10.1016/j.apcatb.2018.11.016

Dan, M., Xiang, J., Wu, F., Yu, S., Cai, Q., Ye, L., et al. (2019b). Rich active-edge-site MoS_2 anchored on reduction sites in metal sulfide heterostructure: toward robust visible light photocatalytic hydrogen sulphide splitting. *Appl. Catal. B Environ.* 256:117870. doi: 10.1016/j.apcatb.2019.117870

Dan, M., Zhang, Q., Yu, S., Prakash, A., Lin, Y., and Zhou, Y. (2017). Noble-metal-free MnS/In_2S_3 composite as highly efficient visible light driven photocatalyst for H_2 production from H_2S. *Appl. Catal. B Environ.* 217, 530–539. doi: 10.1016/j.apcatb.2017.06.019

Gao, C., Zhang, Z., Li, X., Chen, L., Wang, Y., He, Y., et al. (2015). Synergistic effects in three-dimensional SnO_2/TiO_2/CdS multi-heterojunction structure for highly efficient photoelectrochemical hydrogen production. *Sol. Energ. Mat. Sol. C* 141, 101–107. doi: 10.1016/j.solmat.2015.05.026

Ge, H., Xu, F., Cheng, B., Yu, J., and Ho, W. (2019). S-scheme heterojunction TiO_2/CdS nanocomposite nanofiber as H_2-production photocatalyst. *ChemCatChem* 11, 6301–6309. doi: 10.1002/cctc.201901486

Kibsgaard, J., Chen, Z., Reinecke, B. N., and Jaramillo, T. F. (2012). Engineering the surface structure of MoS_2 to preferentially expose active edge sites for electrocatalysis. *Nat. Mater.* 11, 963–969. doi: 10.1038/nmat3439

Kresse, G., and Furthmüller, J. (1996). Efficient iterative schemes for ab initio total-energy calculations using a plane-wave basis set. *Phys. Rev. B* 54, 11169–11186. doi: 10.1103/PhysRevB.54.11169

Kresse, G., and Joubert, D. (1999). From ultrasoft pseudopotentials to the projector augmented-wave method. *Phys. Rev. B* 59 1758–1775. doi: 10.1103/PhysRevB.59.1758

Li, X., Lv, X., Li, N., Wu, J., Zheng, Y., and Tao, X. (2019). One-step hydrothermal synthesis of high-percentage 1T-phase MoS_2 quantum dots for remarkably enhanced visible-light-driven photocatalytic H_2 evolution. *Appl. Catal. B Environ.* 243, 76–85. doi: 10.1016/j.apcatb.2018.10.033

Li, Y., Hong, H., Xue, X., Zhang, Z., and Tian, H. (2019). MoS_2 as cocatalyst for improving photocatalytic performance of Bi_2MoO_6, *ChemistrySelect* 4, 5222–5227. doi: 10.1002/slct.201900016

Li, Y., Wang, H., Xie, L., Liang, Y., Hong, G., and Dai, H. (2011). MoS_2 nanoparticles grown on graphene: an advanced catalyst for the hydrogen evolution reaction. *J. Am. Chem. Soc.* 133, 7296–7299. doi: 10.1021/ja201269b

Lin, Y., Shi, H., Jiang, Z., Wang, G., Zhang, X., Zhu, H., et al. (2017). Enhanced optical absorption and photocatalytic H_2 production activity of g-C_3N_4/TiO_2 heterostructure by interfacial coupling: a DFT+U study. *Int. J. Hydrogen Energ.* 42, 9903–9913. doi: 10.1016/j.ijhydene.2017.02.172

Liu, B., Liu, X., Liu, J., Feng, C., Li, Z., Li, C., et al. (2018). Efficient charge separation between UiO-66 and $ZnIn_2S_4$ flowerlike 3D microspheres for photoelectronchemical properties. *Appl. Catal. B Environ.* 226, 234–241. doi: 10.1016/j.apcatb.2017.12.052

Liu, L., Gu, X., Cao, Y., Yao, X., Zhang, L., Tang, C., et al. (2013). Crystal-plane effects on the catalytic properties of Au/TiO_2. *ACS Catal.* 3, 2768–2775. doi: 10.1021/cs400492w

Liu, Q., Li, X., He, Q., Khalil, A., Liu, D., Xiang, T., et al. (2015). Gram-scale aqueous synthesis of stable few-layered 1T-MoS_2: applications for visible-light-driven photocatalytic hydrogen evolution. *Small* 11, 5556–5564. doi: 10.1002/smll.201501822

Liu, Q., Pu, Z., Asiri, A. M., Qusti, A., Al-youbi, A., and Sun, X. (2013). One-step solvothermal synthesis of MoS_2/TiO_2 nanocomposites with enhanced photocatalytic H_2 production. *J. Nanopart. Res.* 15, 2057–2064. doi: 10.1007/s11051-013-2057-8

Liu, X., Liu, B., Li, L., Zhuge, Z., Chen, P., Li, C., et al. (2019). $Cu_2In_2ZnS_5$/Gd_2O_2S:Tb for full solar spectrum photoreduction of Cr(VI) and CO_2 from UV/vis to near-infrared light. *Appl. Catal. B Environ.* 249, 82–90. doi: 10.1016/j.apcatb.2019.02.061

Liu, X., Xing, Z., Zhang, Y., Li, Z., Wu, X., Tan, S., et al. (2017). Fabrication of 3D flower-like black N-TiO_{2-x}@MoS_2 for unprecedented-high visible-light-driven photocatalytic performance. *Appl. Catal. B Environ.* 201, 119–127. doi: 10.1016/j.apcatb.2016.08.031

Liu, X., Zhang, H., Yao, X., An, T., Liu, P., Wang, Y., et al. (2012). Visible light active pure rutile TiO_2 photoanodes with 100% exposed pyramid-shaped (111) surfaces. *Nano Res.* 5, 762–769. doi: 10.1007/s12274-012-0259-5

Ren, Z., Liu, X., Zhuge, Z., Gong, Y., and Sun, C. (2020). $MoSe_2$/ZnO/ZnSe hybrids for efficient Cr (VI) reduction under visible light irradiation. *Chin. J. Catal.* 41, 180–187. doi: 10.1016/S1872-2067(19)63484-4

Rybolt, T. R., Wells, C. E., Sisson, C. R., Black, C. B., and Ziegler, K. A. (2007). Evaluation of molecular mechanics calculated binding energies for isolated and monolayer organic molecules on graphite. *J. Colloid Interface Sci.* 314, 434–445. doi: 10.1016/j.jcis.2007.05.083

Sharma, A., Liu, N., Ma, Q., Zheng, H., Kawazoe, N., Chen, G., et al. (2020). PEG assisted P/Ag/Ag_2O/Ag_3PO_4/TiO_2 photocatalyst with enhanced elimination of emerging organic pollutants in salinity condition under solar light illumination. *Chem. Eng. J.* 385:123765. doi: 10.1016/j.cej.2019.123765

Shuxian, Z., Hall, W. K., Ertl, G., and Knözinger, H. (1986). X-ray photoemission study of oxygen and nitric oxide adsorption on MoS_2. *J. Catal.* 100, 167–175. doi: 10.1016/0021-9517(86)90082-5

Song, S., Wang, J., Peng, T., Fu, W., and Zan, L. (2018). MoS_2-MoO_{3-x} hybrid cocatalyst for effectively enhanced H_2 production photoactivity of $AgIn_5S_8$ nano-octahedrons. *Appl. Catal. B Environ.* 228, 39–46. doi: 10.1016/j.apcatb.2018.01.077

Sun, J., Duan, L., Wu, Q., and Yao, W. (2018). Synthesis of MoS_2 quantum dots cocatalysts and their efficient photocatalytic performance for hydrogen evolution. *Chem. Eng. J.* 332, 449–455. doi: 10.1016/j.cej.2017.09.026

Tang, C., Xu, W., Chen, C., Li, Y., and Xu, L. (2017). Unraveling the orientation of MoS_2 on TiO_2 for photocatalytic water splitting. *Adv. Mater. Interfaces* 4, 1700361–1700367. doi: 10.1002/admi.201700361

Toroker, M. C., Kanan, D. K., Alidoust, N., Isseroff, L. Y., Liao, P., and Carter, E. A. (2011). First principles scheme to evaluate band edge positions in potential transition metal oxide photocatalysts and photoelectrodes. *Phys. Chem. Chem. Phys.* 13, 16644–16654. doi: 10.1039/c1cp22128k

Wang, Y., Liu, J., Ozaki, Y., Xu, Z., and Zhao, B. (2019). Effect of TiO_2 on altering direction of interfacial charge transfer in a TiO_2-Ag-MPY-FePc system by SERS. *Angew. Chem. Int. Edit.* 58, 8172–8176. doi: 10.1002/anie.201900589

Wang, Y., Sun, T., Yang, D., Liu, H., Zhang, Z., Yao, X., et al. (2012). Structure, reactivity, photoactivity and stability of Ti–O based materials: a theoretical comparison. *Phys. Chem. Chem. Phys.* 14, 2333–2338. doi: 10.1039/c2cp23143c

Woo, H. C., Nam, I., Lee, J. S., Chung, J. S., Lee, K. H., and Kim, Y. G. (1992). Room-temperature oxidation of $K_2CO_3MoS_2$ catalysts and its effects on alcohol synthesis from CO and H_2. *J. Catal.* 138, 525–535. doi: 10.1016/0021-9517(92)90304-Z

Xiang, J., Dan, M., Cai, Q., Yu, S., and Zhou, Y. (2019). Graphene oxide induced dual cocatalysts formation on manganese sulfide with enhanced photocatalytic hydrogen production from hydrogen sulfide. *Appl. Surf. Sci.* 494, 700–707. doi: 10.1016/j.apsusc.2019.07.219

Yang, Y. (2018). Comparative study of low-index {101}-TiO_2, {001}-TiO_2, {100}-TiO_2 and high-index {201}-TiO_2 on glyphosate adsorption and photodegradation. *Chem. Eng. J.* 360:1247. doi: 10.1016/j.cej.2018.10.219

Yang, Y., Ye, K., Cao, D., Gao, P., Qiu, M., Liu, L., et al. (2018). Efficient charge separation from F^- selective etching and doping of anatase-TiO_2 {001} for enhanced photocatalytic hydrogen production. *ACS Appl. Mater. Interfaces* 10, 19633–19638. doi: 10.1021/acsami.8b02804

Yu, H., Yuan, R., Gao, D., Xu, Y., and Yu, J. (2019). Ethyl acetate-induced formation of amorphous MoS_x nanoclusters for improved H_2-evolution activity of TiO_2 photocatalyst. *Chem. Eng. J.* 375:121934. doi: 10.1016/j.cej.2019.121934

Yu, S., Zhong, Y., Yu, B., Cai, S., Wu, L., and Zhou, Y. (2016). Graphene quantum dots to enhance the photocatalytic hydrogen evolution efficiency of anatase TiO_2 with exposed {001} facet. *Phys. Chem. Chem. Phys.* 18, 20338–20344. doi: 10.1039/C6CP02561G

Yuan, Y., Ye, Z., Lu, H., Hu, B., Li, Y., Chen, D., et al. (2016). Constructing anatase TiO_2 nanosheets with exposed (001) facets/layered MoS_2 two-dimensional nanojunctions for enhanced solar hydrogen generation. *ACS Catal.* 6, 532–541. doi: 10.1021/acscatal.5b02036

Zeng, F., Li, N., Shen, Y., Zhou, X., Jin, Z., Yuan, N., et al. (2019). Improve the electrodeposition of sulfur and lithium sulfide in lithium-sulfur batteries with a comb-like ion-conductive organo-polysulfide polymer binder. *Energy Storage Mater.* 18, 190–198. doi: 10.1016/j.ensm.2018.09.018

Zhang, N., Ma, W., Wu, T., Wang, H., Han, D., and Niu, L. (2015). Edge-rich MoS_2 naonosheets rooting into polyaniline nanofibers as effective catalyst for electrochemical hydrogen evolution. *Electrochim. Acta* 180, 155–163. doi: 10.1016/j.electacta.2015.08.108

Zhang, R., Wan, W., Li, D., Dong, F., and Zhou, Y. (2017). Three-dimensional MoS_2/reduced graphene oxide aerogel as a macroscopic visible-light photocatalyst. *Chin. J. Catal.* 38, 313–320. doi: 10.1016/S1872-2067(16)62568-8

Zhang, Y., Guo, S., Xin, X., Song, Y., Lin, Y., Wang, B., et al. (2020). Plasmonic MoO2 as co-catalyst of MoS2 for enhanced photocatalytic hydrogen evolution. *Appl. Surf. Sci.* 504:144291. doi: 10.1016/j.apsusc.2019.144291

Zhao, M., Xu, H., Ouyang, S., Tong, H., Chen, H., Li, Y., et al. (2018). Fabricating a Au@TiO_2 plasmonic system to elucidate alkali-induced enhancement of photocatalytic H_2 evolution: surface potential shift or methanol oxidation acceleration? *ACS Catal.* 8, 4266–4277. doi: 10.1021/acscatal.8b00317

Zhou, W., Yin, Z., Du, Y., Huang, X., Zeng, Z., Fan, Z., et al. (2013). Synthesis of few-layer MoS_2 nanosheet-coated TiO_2 nanobelt heterostructures for enhanced photocatalytic activities. *Small* 9, 140–147. doi: 10.1002/smll.201201161

Conflict of Interest: The authors declare that the research was conducted in the absence of any commercial or financial relationships that could be construed as a potential conflict of interest.